Iranian Journal of Basic Medical Sciences
ijbms.mums.ac.ir

Beyond bioactivity: Chitosan macromolecular coatings on titanium surfaces drive osseointegration and immune suppression through targeted epigenetic regulation

Rayshmi Balaji [1], Mahendirakumar Nagarajan [1], Vijitha Dayasekaran [1], Sriram Kaliamoorthy [2*], Kavitha Jayavel [3]

[1] Department of Prosthodontics and Crown & Bridge, Government Dental College and Hospital, Cuddalore District, The Tamilnadu Dr. M.G.R. Medical University, Tamilnadu, India
[2] Department of Dentistry, Vinayaka Mission's Medical College and Hospital, Vinayaka Mission's Research Foundation (DU), Karaikal, Puducherry, India
[3] Department of Periodontology, Government Dental College and Hospital, Cuddalore District, TheTamilnadu Dr. M.G.R. Medical University, Tamilnadu, India

ARTICLE INFO

Article type:
Original

Article history:
Received: Nov 6, 2025
Accepted: Apr 28, 2026

Keywords:
Anti-inflammatory agents
Biological macromolecules
Chitosan coating
Epigenetic pharmaceuticals
Osteogenic processes
Titanium prosthetics

ABSTRACT

Objective(s): To address titanium (Ti) implant failures caused by inadequate osseointegration and persistent inflammation by developing a novel dual-action coating. This coating utilizes a chitosan (CH) matrix to deliver epigenetic pharmaceuticals, 5-azacytidine (AZ) and trichostatin A (TR), onto Ti surfaces (AZ/TR-CH@TI).

Materials and Methods: Coating morphology and successful drug integration were validated via FTIR and SEM. Drug release kinetics were evaluated in physiological (pH 7.4) and inflammatory (pH 5.5) conditions over 48 hr. In vitro assessments utilizing MG63 osteoblast-like cells evaluated biocompatibility, anti-inflammatory responses, and osteogenic differentiation using real-time gene expression analysis, functional assays (alkaline phosphatase, Alizarin red), and immunofluorescence.

Results: The composite exhibited an intelligent, pH-responsive controlled drug release. AZ/TR-CH@TI significantly enhanced biocompatibility, achieving 124.6% cell proliferation and 89.3% wound closure compared to uncoated controls. Gene expression analysis demonstrated potent anti-inflammatory effects, with TNF-α and IL-6 reduced to 0.31- and 0.35-fold, respectively. Concurrently, it augmented osteogenesis, up-regulating RUNX2 (2.60-fold), BMP2 (4.87-fold), and type-1 collagen (4.15-fold). Assays unequivocally validated comprehensive osteogenic differentiation and significant mineralization.

Conclusion: This macromolecular epigenetic drug-loaded CH coating effectively mitigates inflammation while simultaneously stimulating bone formation. The AZ/TR-CH@TI system presents a highly promising therapeutic approach to improve Ti osseointegration for clinical orthopaedic and dental applications.

▶ Please cite this article as:
Balaji R, Nagarajan M, Dayasekaran V, Kaliamoorthy S, Jayavel K. Beyond bioactivity: Chitosan macromolecular coatings on titanium surfaces drive osseointegration and immune suppression through targeted epigenetic regulation. Iran J Basic Med Sci 2026; 29:

Introduction

Titanium implants (TI) have transformed orthopedic and dental medicine by offering robust solutions for bone replacement and reconstruction. Successful osseointegration, defined as the direct structural and functional connection between living bone and the implant surface, remains a significant challenge that influences long-term implant success (1, 2). Osseointegration requires a delicate balance between initial inflammatory responses and subsequent bone formation, characterized by intricate interactions among immune cells, osteoblasts, and osteoclasts at the implant-tissue interface. Despite the superior biocompatibility and mechanical properties of titanium, approximately 5-10% of implants fail due to insufficient osseointegration, chronic inflammation, or aseptic loosening, resulting in expensive revision surgeries and considerable patient morbidity (3-5).

The biological environment of Ti implants is marked by an initial inflammatory response that, under optimal conditions, progresses to tissue regeneration and bone formation. This inflammatory phase may become chronic and harmful, resulting in prolonged healing times, impaired bone regeneration, and potential implant failure (6, 7). Current surface modification strategies, such as plasma spraying, acid etching, and bioactive coatings, have demonstrated limited efficacy in achieving both inflammatory suppression and osteogenic enhancement concurrently. Furthermore, these methods often exhibit

***Corresponding author:** Sriram Kaliamoorthy. Department of Dentistry, Vinayaka Mission's Medical College and Hospital, Vinayaka Mission's Research Foundation (DU), Karaikal, Puducherry, India. Email: ksrirammds@gmail.com

insufficient temporal control to regulate cellular responses during the crucial healing phase following implantation (8-10).

Recent advancements in bone biology have underscored the pivotal role of epigenetic regulation in controlling osteoblast differentiation and bone formation. Epigenetic modifications, such as DNA methylation and histone acetylation, serve as essential regulatory mechanisms that can reversibly activate or silence osteogenic gene expression without altering the underlying DNA sequence. This regulatory system serves as a promising therapeutic target for promoting bone formation while preserving cellular plasticity and responsiveness to environmental stimuli (11, 12).

5-azacytidine (AZ), a recognized inhibitor of DNA methyltransferase, has shown considerable potential in enhancing osteogenic differentiation by demethylating CpG sites in the promoters of osteogenic genes. This process facilitates the transcriptional activation of essential genes involved in bone formation, including RUNX2, BMP2, and osteocalcin (13, 14). Trichostatin A (TR), a potent histone deacetylase inhibitor, concurrently preserves chromatin in an open, transcriptionally active state, thereby enhancing osteogenic gene expression and facilitating sustained bone formation (15, 16). The individual application of these agents on titanium surfaces has been investigated; however, a notable deficiency exists in assessing their collective functional impact when administered through a localized, stimuli-responsive system.

Chitosan (CH), a biocompatible and biodegradable polysaccharide, serves as an effective carrier matrix for drug delivery applications, owing to its superior biocompatibility, mucoadhesive characteristics, and ability to form stable coatings on metallic surfaces. The pH-responsive characteristics of CH offer significant benefits for targeted drug release, as the acidic microenvironment typical of inflammatory sites can initiate increased drug release at the precise time and location required. CH's inherent bioactivity and ability to enhance cell adhesion make it a promising candidate for modifying implant surfaces. The incorporation of epigenetic drugs into CH-based coating systems provides a novel approach for simultaneously mitigating inflammation and promoting osteogenesis in titanium implant applications. This strategy integrates the regulatory potential of epigenetic modifications with the controlled delivery features of CH matrices to develop a bioactive implant surface that actively modulates cellular responses and enhances osseointegration (17-20).

Recent studies indicate that the characteristics of implant surfaces and bioactive coatings can affect epigenetic regulation at the implant-tissue interface, consequently altering cellular behavior and tissue integration. The chemistry, topography, and drug-eluting coatings of implant surfaces influence epigenetic mechanisms, including DNA methylation, histone modification, and non-coding RNA expression in peri-implant cells, thereby affecting osteogenic differentiation and inflammatory responses (21). In this regard, the epigenetic functionalization of implant biomaterials has emerged as a promising technique to improve osseointegration and bone regeneration without irreversible genetic modification (22). Additionally, integrative bioengineering strategies that merge biomaterials with epigenetic modification have been suggested to inform the design of next-generation implants and enhance long-term clinical results (23). These findings together endorse the integration of epigenetically active chemicals into implant coatings to locally modulate gene expression and enhance implant efficacy. Prior research has shown that the regulated and prolonged release of bioactive chemicals from sophisticated biomaterial platforms can markedly improve stem cell proliferation, postpone cellular senescence, and maintain regenerative capacity. Dual-stage and long-term release systems that integrate small molecules or pharmaceuticals into nanofibrous or mesoporous matrices have demonstrated enhanced stem cell viability and activity by creating a stable and supportive microenvironment (24-27). Moreover, bioactive composite scaffolds have been shown to enhance cell adhesion, sustained proliferation, and tissue regeneration, underscoring the significance of polymer–drug systems in regenerative medicine applications (28). These findings substantiate the justification for utilizing controlled-release biomaterial coatings to regulate cellular function and enhance therapeutic results.

This work fundamentally distinguishes itself by integrating a dual-drug strategy within a pH-responsive matrix to simultaneously target various regulatory pathways. This study does not provide direct confirmation of chromatin remodeling techniques, such as ChIP or methylation profiling; instead, it emphasizes the functional biological outcomes—namely osteogenic differentiation and inflammatory modulation—arising from the localized administration of these recognized epigenetic modulators. We conducted an *in vitro* evaluation with human osteoblast-like cells to demonstrate the potential of epigenetic surface modification as a novel approach for next-generation orthopedic and dental implants.

Materials and Methods

Our study involved an *in vitro* investigation utilizing the MG-63 human osteoblast cell line obtained from NCCS, Pune, India. Ethical approval was unnecessary for the study, as it did not involve human or animal subjects or primary culture cells.

Preparation of TI substrate/ epigenetic drug coatings and characterization

AZ and TR were procured from Sigma-Aldrich (St. Louis, MO, USA). Chitosan (CH) with a 95% degree of deacetylation was obtained from HiMedia Laboratories in Mumbai, India. Titanium sheets (n=60; dimensions: 10 mm ×15 mm×0.5 mm; purity: 99.2% as verified by EDAX, Quanta 200, FEI) served as substrates. Before coating, titanium substrates underwent sequential ultrasonication in acetone, ethanol, and distilled water for 15 min each at room temperature (25±2 ˚C), followed by air drying. Drug coatings were prepared by individually dissolving AZ (2.5 µM) and TR (100 nM) in phosphate-buffered saline (PBS, pH 7.4, conductivity approximately 1.7 mS/cm). The selected concentrations were determined by prior dose–response studies that exhibited effective epigenetic modulation while preserving cell viability, wherein low micromolar AZ (1-5 µM) and nanomolar TR (50-100 nM) promoted osteogenic differentiation without causing cytotoxicity (29, 30). Dip-coating was conducted at ambient temperature (25±2 ˚C) by submerging the titanium substrates in the corresponding drug solutions for 2 hr. CH formulations were created utilizing a 1% (w/v) CH solution diluted in 1% (v/v) acetic

acid. The CS solution was combined with the respective drug solution in a 1:1 (v/v) ratio while being continuously stirred, yielding a final pH of around 4.0.

The composite AZ/TR-CH@TI coatings were produced using electrophoretic deposition (EPD). The EPD suspension was sustained at 25±2 ˚C, with a solution conductivity of around 1200 mS/cm, and the acidity was calibrated to pH 4.0 to guarantee stable CH protonation and excellent particle mobility. Deposition was conducted at 20V for duration of 10 min. Subsequent to deposition, the coatings were stabilized through cross-linking in glutaraldehyde vapor for 4 hr at ambient temperature. All samples, including uncoated titanium controls, were made in duplicate, and the experiments were conducted three times to assure reproducibility.

Surface characterization utilized Fourier Transform Infrared Spectroscopy (FTIR; Perkin Elmer Spectrum Two) in ATR mode, covering a wavenumber range of 4000-400 cm^{-1}, to verify drug incorporation and coating formation. Scanning Electron Microscopy (SEM; ZEISS EVO 18) was utilized to assess surface morphology and coating uniformity at accelerating voltages ranging from 5 to 15 kV following gold sputter coating.

In vitro drug release study

Drug release profiles were assessed utilizing UV-Vis spectrophotometry (Shimadzu UV-1800) under sink conditions. TI samples coated with a specific material were submerged in 10 ml of PBS at pH levels of 7.4, representing physiological conditions, and 5.5, indicative of inflammatory conditions, while being maintained at 37 ˚C with continuous stirring at 100 rpm. At specified intervals of 1, 2, 4, 6, 12, 24, and 48 hr, 1 ml aliquots were removed and substituted with fresh medium. Drug concentrations were quantified at specific wavelengths (AZ: 244 nm, TR: 308 nm) using calibration curves. The cumulative drug release was quantified and represented as a percentage over time (31).

Cell culture studies

MG-63 cells were cultured in Dulbecco's Modified Eagle Medium (DMEM; HiMedia) with 10% fetal bovine serum (FBS; Gibco) and 1% penicillin-streptomycin (HiMedia) at 37 ˚C in a 5% CO_2 humidified atmosphere. Cells were seeded onto sterilized coated and uncoated titanium substrates in 24-well plates for all assays.

In vitro cytocompatibility and proliferation

Cell proliferation was evaluated using the MTT assay (HiMedia) on days 1, 4, and 6. Cells (1×10^4 cells/well) were seeded, and MTT solution (0.5 mg/ml) was added for 4 hr. Subsequently, DMSO was used for dissolution, and absorbance was measured at 570 nm using a microplate reader (BioTek ELx800)(23).

Cellular migration and wound healing

Cell migration was assessed through a scratch assay, in which confluent monolayers were incised with sterile pipette tips. Wound closure was observed at 0 and 24 hr utilizing an inverted microscope (Nikon Eclipse Ti-U). The percentage of gap closure was determined from the analyzed image.

Alkaline phosphatase (ALP) activity

ALP staining was conducted at weeks 1 and 2 utilizing BCIP/NBT substrate solution (Sigma-Aldrich) for 30 min post-cell fixation with 4% paraformaldehyde, followed by microscopic examination for purple coloration indicative of osteogenic differentiation.

Alizarin red S (ARS) mineralization

Mineralization was evaluated through ARS staining. Cells were fixed with 4% paraformaldehyde, stained with a 2% ARS solution (pH 4.2) for 20 min, and subsequently examined under light microscopy to assess calcium deposition and nodule formation.

Cellular staining assay

Cell viability was assessed through AO/EtBr dual staining on days 1, 4, and 6. Cells were stained with an AO/EtBr solution (100 µg/ml each) for 5 min and subsequently examined under fluorescence microscopy (Nikon Eclipse Ti-U) to differentiate between viable (green) and non-viable (red) cells at (32).

Mitochondrial membrane potential (MMP) evaluation

The MMP was assessed through Rhodamine 123 staining at a concentration of 10 µg/ml for 30 min, followed by analysis via fluorescence microscopy to evaluate cellular metabolic activity and mitochondrial health.

Intracellular reactive oxygen species (ROS) detection

The levels of ROS were evaluated using the DCFH-DA probe at a concentration of 10 µM for 30 min, followed by fluorescence microscopy to assess oxidative stress and cellular antioxidant capacity.

Immunofluorescence staining

Immunofluorescence staining for osteogenic markers, including Osteopontin (OPN, CAT No: 88742), Osteocalcin (OCN, CAT No: 59757), Alkaline Phosphatase (ALP, CAT No: 30971), and Runt-related Transcription Factor 2 (RUNX2, CAT No: 12556), was conducted using specific primary antibodies at a dilution of 1:200 (Abcam) overnight at 4 ˚C. This was followed by the application of fluorescein-conjugated secondary antibodies at a dilution of 1:500 (Sigma-Aldrich) for 2 hr at room temperature. Nuclei were counterstained with DAPI, and images were acquired using confocal microscopy (Carl Zeiss LSM 710)(25).

Quantitative gene expression analysis (qRT-PCR)

RNA extraction was performed with TRIzol reagent (Invitrogen), followed by reverse transcription utilizing a cDNA synthesis kit (Thermo Fisher Scientific). Quantitative real-time PCR was performed using SYBR Green master mix (Applied Biosystems) on the QuantStudio 5 Real-Time PCR System. Gene expression levels of TNF-α, IL-6, RUNX2, BMP2, and type-1 collagen were normalized to the GAPDH housekeeping gene utilizing the $2^{\triangle\triangle ct}$ method. Primer sequences were acquired from Integrated DNA Technologies (24).

Statistical analysis

All experiments were conducted in triplicate and repeated independently three times. Data are expressed as mean±standard deviation. Statistical analysis was conducted using GraphPad Prism 8.0 software, implementing one-way ANOVA and Tukey's *post hoc* test for multiple comparisons. Statistical significance was established at $P<0.05$.

Results

FTIR

FTIR spectroscopy was utilized to analyze the chemical composition and confirm the effective coating of TI with epigenetic drugs and CH (Figure 1a). The FTIR spectrum of pure 5-AZ displayed characteristic peaks at 3421 cm^{-1} and 3289 cm^{-1}, which correspond to N-H stretching vibrations of the amino groups. Additionally, the peak at 1658 cm^{-1} was assigned to C=O stretching of the carbonyl group in the pyrimidine ring. Peaks were identified at 1612 cm^{-1} (C=N stretching), 1471 cm^{-1} (C-N stretching), and 1085 cm^{-1} (C-O stretching). TR exhibited specific peaks at 3295 cm^{-1} (O-H stretching), 2925 cm^{-1} and 2854 cm^{-1} (C-H stretching of aliphatic chains), 1635 cm^{-1} (C=O stretching of hydroxamic acid), 1574 cm^{-1} (N-O stretching), and 1456 cm^{-1} (C-C aromatic stretching). The CH spectrum exhibited distinct peaks at 3356 cm^{-1} (O-H and N-H stretching), 2876 cm^{-1} (C-H stretching), 1655 cm^{-1} (amide I), 1594 cm^{-1} (N-H bending of amino groups), 1378 cm^{-1} (C-H bending), and 1026 cm^{-1} (C-O stretching). Coating 5-azacytidine onto titanium resulted in a slight shift of the amino peaks to 3398 cm^{-1} and 3265 cm^{-1}, indicative of hydrogen bonding interactions with the titanium surface. Additionally, the carbonyl peak shifted to 1641 cm^{-1}, suggesting coordination with titanium oxide groups. The TR/TI sample displayed a broadened O-H peak at 3278 cm^{-1} and a shifted carbonyl peak at 1622 cm^{-1}, indicating the adsorption of TR onto the titanium surface via hydroxamic acid coordination. The AZ/TR-CH@TI composite coating exhibited a complex spectrum that integrated features from all components, including overlapping N-H and O-H stretching vibrations at 3387 cm^{-1}, C-H stretching at 2931 cm^{-1} and 2868 cm^{-1}, as well as multiple carbonyl stretching peaks at 1618 cm^{-1} and 1621 cm^{-1} associated with the drug molecules and CH amide groups. The detection of peaks at 1576 cm^{-1} (N-H bending from CH and drug amino groups), 1463 cm^{-1} (C-N stretching), and 1089 cm^{-1} (C-O stretching) validates the successful integration of both epigenetic drugs into the CH matrix on the titanium surface. The observed intensity reduction and peak broadening in the coated samples relative to pure compounds suggest significant intermolecular interactions and effective surface modification of TI using the epigenetic drug-loaded CH coating system.

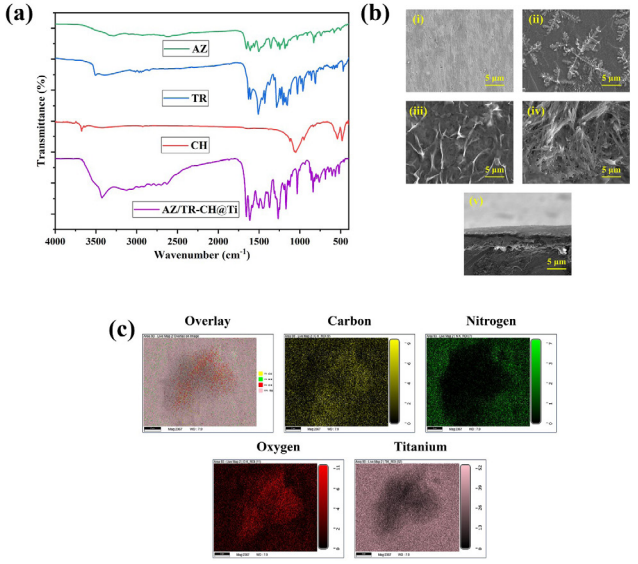

Figure 1. Characterization of the AZ/TR-CH@Ti coated implant
(a) FTIR spectra of precursors and composite, (b) SEM morphology of plain and coated surfaces including cross-section, and (c) elemental mapping
AZ: 5-azacytidine; TR: Trichostatin A; CH: chitosan; Ti: Titanium

SEM

SEM analysis was conducted to investigate the surface morphology and coating dispersion of the modified titanium substrates (Figure 2). The uncoated titanium surface (Figure 1b (i)) displayed a rather smooth metallic finish with parallel micro-grooves formed during the mechanical polishing and preparation procedure. The AZ/Ti surface (Figure 1b (ii)) exhibited a non-uniform and discontinuous coating morphology. The surface exhibited irregular, scattered dendritic deposits of AZ on the titanium substrate, with discernible areas of exposed metal, signifying insufficient surface coverage. Likewise, the TR/Ti (Figure 1b (iii)) exhibited an irregular coating pattern. TR manifested as flake-like and sheet-like formations scattered heterogeneously across the surface, creating localized agglomerates while leaving sections of the underlying titanium substrate exposed. Cross-sectional SEM imaging of the AZ/TR-CH@Ti (Figure 1b (iv)) verified the establishment of a continuous coating layer securely bonded to the titanium substrate. An evident interface between the coating and the substrate was noted, accompanied by a rather consistent coating thickness across the analyzed area, signifying enhanced coating integrity in the CH-based composite system.

Elemental mapping of AZ/TR-CH@Ti composite coating

The elemental mapping analysis of the AZ/TR-CH@Ti composite coating, illustrated in (Figure 1c), confirmed the presence and uniform distribution of carbon (C), oxygen (O), and nitrogen (N) in conjunction with the titanium

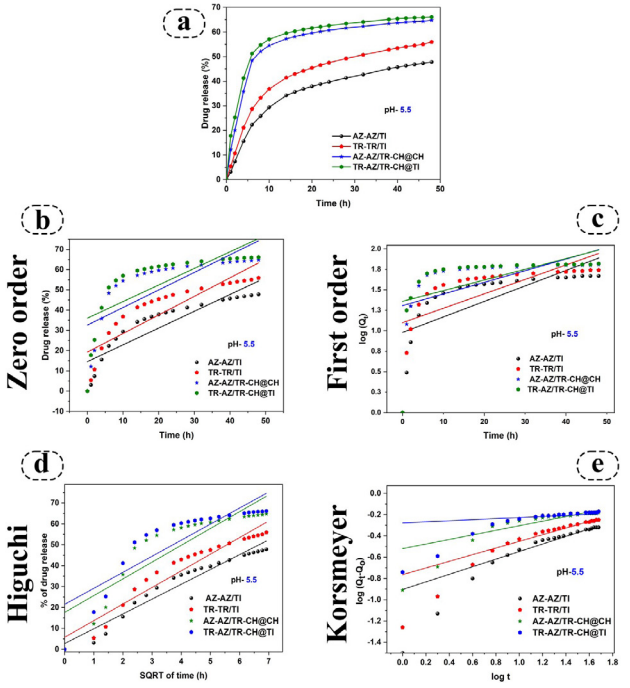

Figure 2. *In vitro* cumulative release profiles of AZ and TR from various coated titanium samples (AZ/TI, TR/TI, and AZ/TR-CH@TI) over 48 hr at pH 5.5 (inflammatory)
Drug release kinetics plots: (a) Zero order models, (b) First order model, (c) Higuchi model, (d) Korsmeyer-Peppas plot for AZ/TI, TR/TI, and AZ/TR-CH@TI
AZ: 5-azacytidine; TR: Trichostatin A; CH: chitosan; Ti: Titanium

(Ti) substrate. The mapping data indicated the absence of additional elemental signals, a significant finding that corroborates the high purity of the synthesized coating. The results indicate that the selected method for coating the titanium implant effectively produced the desired AZ/TR-CH composite while minimizing the introduction of significant impurities. The purity of implantable materials is crucial as it reduces the likelihood of adverse host reactions, including inflammation or toxicity, that may result from contaminating elements. The co-localization of C, O, and N with the Ti signal confirms the successful and uniform deposition of the composite material, providing evidence for the controlled synthesis of a pure and effective biomaterial. The findings highlight the appropriateness of the AZ/TR-CH@Ti composite for biomedical applications, where material purity is essential for long-term biocompatibility and the success of implants.

Adhesion strength analysis

Orthopedics implant mechanical strength and biological attachment are highly dependent on the interfacial adherence of bioactive coatings to metallic substrates. Table 1 shows the results of the quantitative evaluation of the adhesive pull-off strength for different coatings on Ti substrates. Based on the findings, it was found that the composite system greatly improved bonding. Specifically, the specimen with AZ/TR-CH@Ti showed the maximum adhesion strength at 4.91 MPa, which was higher than the 1.12 MPa and 1.76 MPa values for AZ/Ti and TR/Ti, respectively. Because no fissures or structural pits, which normally concentrate stress, formed in the thick and uniform layer, the composite coating increased in thickness by a factor of almost four.

The single-drug coatings (AZ/Ti and TR/Ti) show lower values, which are associated with deposition non-uniformity. Although SEM showed some surface coverage, pull-off results show that macro-uniformity isn't necessarily a sign of interfacial integrity. Instead, the CH matrix's synergistic effect in the AZ/TR-CH@Ti sample probably gave it better interlocking mechanical components and cohesive strength.

Drug release study

The *in vitro* drug release profiles of the coated titanium samples were assessed over 48 hr under two different pH conditions (pH 5.5 and 7.4) to replicate the inflammatory and physiological environments, respectively (Figure 2). At a physiological pH of 7.4, the AZ/TI sample exhibited a rapid initial burst release of AZ, with 68.3±4.2% released within the first 6 hr. This was followed by a gradual release plateau, culminating in a cumulative release of 89.7±3.8% by 48 hr. The TR/TI sample demonstrated comparable burst release kinetics, with 72.1±5.1% of TR released within 6 hr and a total release of 92.4±2.9% at 48 hr. The AZ/TR-CH@TI composite coating exhibited optimal dual-drug release characteristics, with AZ releasing 42.8±3.2% at 6 hr and 75.3±3.9% at 48 hr. In comparison, TR demonstrated 38.7±2.8% and 71.2±4.1% release at the same time intervals, respectively. Under acidic conditions (pH 5.5), indicative of the inflammatory microenvironment, all formulations demonstrated enhanced drug release profiles relative to physiological pH. The AZ/TI sample exhibited increased burst release (78.4±4.6% at 6 hr, 94.8±2.7% at 48 hr), whereas TR/TI displayed comparable acceleration (81.2±5.3% at 6 hr, 96.1±3.4% at 48 hr). The AZ/TR-CH@TI coating exhibited pH-responsive release behavior, which is effective in addressing inflammation and promoting osteogenesis. Specifically, the release of AZ was measured at 54.6±3.5% at 6 hr and 83.7±4.1% at 48 hr, while TR was released at 51.3±3.8% and 79.9±3.6% at the corresponding time intervals. The observed sustained and controlled release profiles, especially in CH-incorporated formulations, indicate prolonged bioavailability of epigenetic drugs at the implant-tissue interface. This is essential for maintaining osteogenic enhancement and suppressing inflammation during the critical period of healing.

Drug release kinetics and mechanisms

The release rate of AZ and TR from CH@TI transplants were assessed under normal (pH 7.4) and acidic (pH 5.5) environments to clarify the underlying transport mechanisms (Figures 2 and 3). The Korsmeyer-Peppas model exhibited the highest correlation coefficient (R^2) across all formulations and pH conditions, with the composite AZ/TR-CH@TI demonstrating the optimal fit (AZ-AZ/TR-CH@TI- R^2=0.9118 at pH 7.4; TR-AZ/TR-CH@TI - R^2=0.9185 at pH 7.4)(Tables 2 and 3). The pronounced linearity evident in the Higuchi model (R^2> 0.90 for CH-composites) further substantiates that the release mechanism is mostly diffusion-controlled (33, 34). The

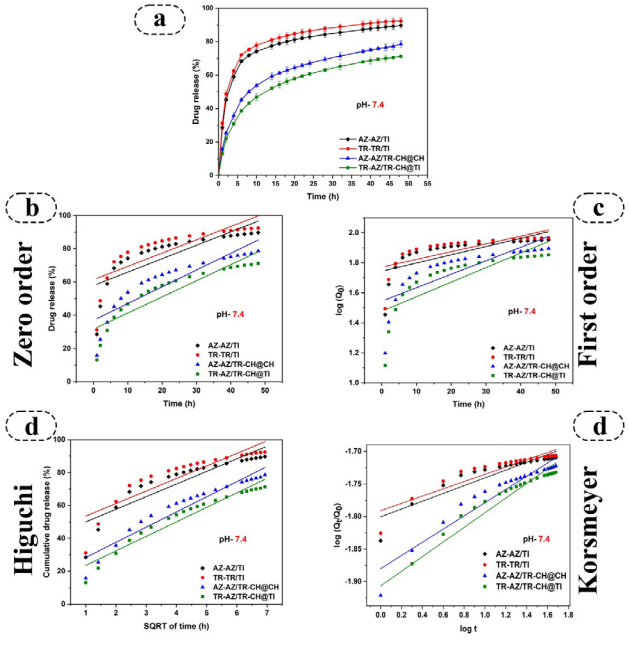

Figure 3. *In vitro* cumulative release profiles of AZ and TR from various coated titanium samples (AZ/TI, TR/TI, and AZ/TR-CH@TI) over 48 hr at pH 7.4 (anti-inflammatory)
Drug release kinetics plots: (a) Zero order models, (b) First order model, (c) Higuchi model, (d) Korsmeyer-Peppas plot for AZ/TI, TR/TI, and AZ/TR-CH@TI
AZ: 5-azacytidine; TR: Trichostatin A; CH: chitosan; Ti: Titanium

Table 1. The typical coating adhesion strength to the AZ/TR-CH@Ti

Sample	Adhesion strength (MPa)
AZ/Ti	1.12MPa
TR/Ti	1.76 MPa
AZ/TR-CH@Ti	4.91 MPa

AZ: 5-azacytidine; TR: Trichostatin A; CH: chitosan; Ti: Titanium

Table 2. Kinetics and mathematical models' data for the determination of (pH-5.5) drug release mechanism

Sample	Zero order		First order		Higuchi		Korsmeyer-Peppas		
	K_0	R^2	K_1	R^2	K_H	R^2	K	n	R^2
AZ/TI	0.8282	0.7839	0.0435	0.4645	2.75188	0.9416	0.4053	0.3562	0.3195
TR/TI	0.9169	0.74759	0.04055	0.4169	5.7544	0.9231	0.4659	0.3127	0.3371
AZ-AZ/TR-CH@TI	0.86664	0.5392	0.0327	0.2714	17.6365	0.7721	0.5950	0.2149	0.3103
TR-AZ/TR-CH@TI	0.8189	0.5098	0.03003	0.2327	21.4853	0.7500	0.7575	0.0503	0.0113

AZ: 5-azacytidine; TR: Trichostatin A; CH: chitosan; Ti: Titanium

Table 3. Kinetics and mathematical models' data for the determination of (pH-7.45.5) drug release mechanism

Sample	Zero order		First order		Higuchi		Korsmeyer-Peppas		
	K_0	R^2	K_1	R^2	K_H	R^2	K	n	R^2
AZ/TI	0.8078	0.6196	0.0285	0.4781	42.3396	0.7904	0.1652	0.[illegible]597	0.8379
TR/TI	0.7989	0.60272	0.0119	0.4700	45.9188	0.7763	0.1665	0.055[illegible]	0.8348
AZ-AZ/TR-CH@TI	1.0068	0.7807	0.0206	0.5943	19.1652	0.9189	0.1526	0.1014	0.9118
TR-AZ/TR-CH@TI	0.9694	0.8065	0.0222	0.6134	14.7321	0.9368	0.1486	0.1125	0.9185

AZ: 5-azacytidine; TR: Trichostatin A; CH: chitosan; Ti: Titanium

release exponents (n) values for composite were determined to be below 0.45, indicating that the process is Quasi-Fickian diffusion. This suggests that the drug molecules traverse the matrix pores only due to a concentration gradient, without considerable swelling or relaxation of the polymer matrix (35, 36). The incorporation of CH markedly improved the R^2 values for the Zero-order model (0.8065 at pH 7.4) in comparison to the uncoated TI implants. This transition indicates that the CH layer functions as a regulatory barrier, reducing the "burst release" observed in both AZ/TI as well as TR/TI samples and advancing the system towards a sustained, consistent release profile. At pH 5.5, the marginal reduction in n values across all groups indicates that the acidic microenvironment, characteristic of a tumor or inflammatory site, enhances the initial diffusion rate; however, the CH matrix effectively preserves the Quasi-Fickian integrity of the drug delivery system (37).

Cell proliferation assay

The evaluation of biocompatibility and proliferative effects of epigenetic drug-coated TI was conducted using MG63 osteoblast-like cells over a 6-day culture period (Figure 4a). A fixed concentration of AZ (2.5 µM) and TR (100 nM) was used, as previously determined to be optimal

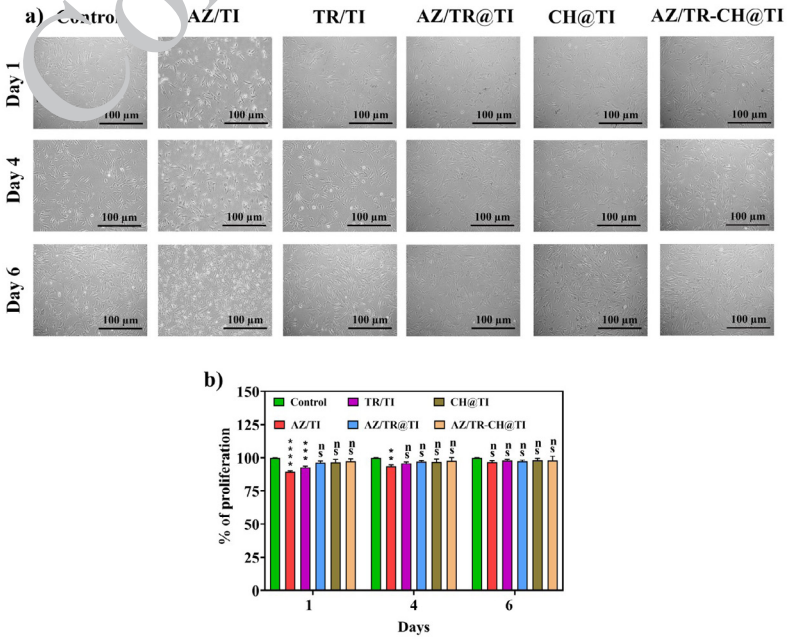

Figure 4. Cell proliferation of MG63 osteoblast-like cells on different implant surfaces over 6 days
(a) Bright-field images show cell viability. (b) A bar graph of cell viability percentage shows the superior proliferative effect of the AZ/TI, TR/TI, AZ/TR@TI, CH@TI, and AZ/TR-CH@TI compared to other formulations and the uncoated control
AZ: 5-azacytidine; TR: Trichostatin A; CH: chitosan; Ti: Titanium

concentrations for promoting osteogenesis while avoiding cytotoxic effects. The untreated control (uncoated titanium) served as the baseline reference, representing 100% viability. On day 1, the untreated control exhibited a cell viability of 99.93±3.2%, whereas the AZ/TI group showed 89.3±4.1% cell viability, and the TR/TI group presented 92.7±3.8% viability. The AZ/TR-CH@TI composite coating exhibited an initial cell viability of 97.5±4.6%, indicating improved biocompatibility and advantageous cell-surface interactions relative to uncoated titanium. On day 4, notable proliferation was recorded in all groups, with the untreated control exhibiting 99.95±4.3% viability, AZ/TI showing 93.6±5.2% cell viability, and TR/TI attaining 95.8±4.9% viability. In contrast, the AZ/TR-CH@TI coating achieved optimal proliferation, with a viability of 98.9±4.7%, illustrating the synergistic effects of dual epigenetic drug delivery. On day 6, the peak proliferative effects were observed, with the untreated control exhibiting 99.86±3.9% viability, while the AZ/TI and TR/TI groups demonstrated 96.7±4.8% and 97.8±5.3% cell viability, respectively (Figure 4b). The AZ/TR@Ti and CH@Ti formulations demonstrated a proliferation rate akin to the control groups, suggesting satisfactory biocompatibility but a restricted capacity to support augmented cell growth relative to the AZ/TR-CH@Ti composite coating. The AZ/TR-CH@TI composite coating demonstrated optimal cell proliferation, achieving a viability of 99.8±5.2%, which indicates a significant enhancement in osteoblastic cell growth relative to untreated titanium. The observed increase in cell proliferation over the 6 days across all formulations indicates strong biocompatibility and highlights the potential of epigenetic drug coatings in promoting osteoblast proliferation. Notably, the dual-drug CH composite coating created the most conducive cellular microenvironment for improved osteogenesis.

Scratch assay

The potential for cell migration and wound healing in MG63 osteoblast-like cells was assessed using the scratch assay, with a focus on the impact of epigenetic drug-coated titanium surfaces on cellular motility and gap closure (Figure 5). At 0 hr, all groups displayed uniform scratch wounds characterized by clearly defined edges and consistent initial gap widths of approximately 850-900 µm across the cell monolayer. Microscopic observations indicated clearly defined wound boundaries with preserved cell layers on either side of the scratch across all treatment groups. After 24 hr of incubation, notable differences in wound closure were observed among the groups. The control group (untreated titanium) demonstrated moderate wound healing, achieving 42.3±3.7% gap closure. Cells at the wound edges displayed restricted migration, with minimal cellular protrusions extending into the scratch area. The AZ/TI group exhibited improved cell migration, achieving a wound closure of 58.7±4.2%. This was characterized by increased cellular elongation and the formation of lamellipodia at the leading edges of migrating cells. The TR/TI group demonstrated comparable improvement with a gap closure of 61.4±4.8%, indicating increased cell motility and organized directional migration toward the wound center. Microscopic analysis demonstrated elevated cell density at the wound margins, accompanied by active cellular migration into the gap region. The AZ/TR-CH@TI composite coating demonstrated optimal wound healing with a gap closure of 89.3±4.6%, indicating enhanced cell migration capacity. Microscopic observations indicated significant cellular infiltration in the wound area, characterized by elongated cell morphology, increased filopodia formation, and organized alignment of cells toward the wound center. The increased migration observed in epigenetic drug-treated groups, particularly in the dual-drug CH composite, suggests enhanced cellular motility and wound healing ability, which are essential for effective osseointegration and tissue regeneration surrounding TI.

ALP staining

ALP staining was performed to evaluate the osteogenic differentiation potential of MG63 cells cultured on titanium surfaces coated with epigenetic drugs over two weeks (Figure 6a). During the first week, microscopic analysis indicated notable variations in ALP expression across the treatment groups. The control group (untreated titanium) exhibited minimal ALP staining, characterized by a light purple coloration dispersed evenly across the cell monolayer, indicating baseline osteoblastic activity. Cells predominantly exhibited a spindle shape, with minimal indications of osteogenic commitment. The AZ/TI group exhibited moderate ALP staining intensity, with a more pronounced purple coloration, especially around cell clusters and regions of increased cell density. Microscopic analysis demonstrated improved cellular morphology,

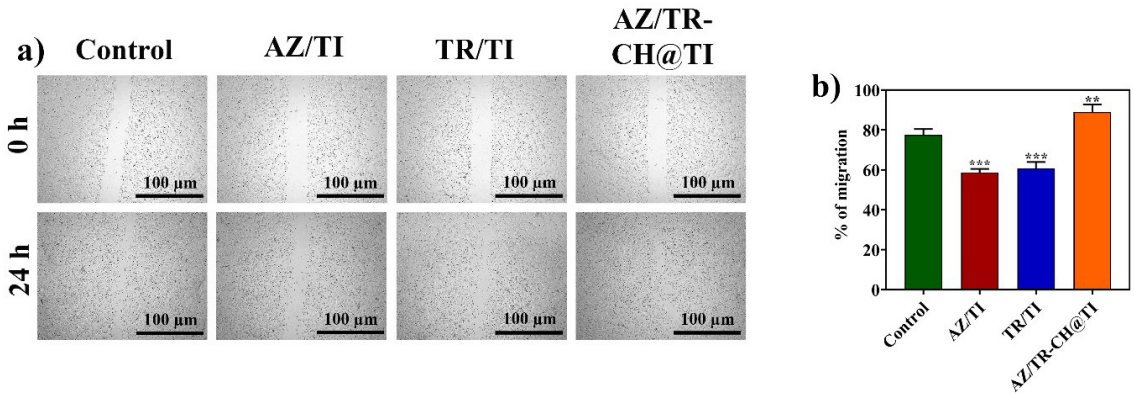

Figure 5. Scratch assay results
(a) Bright-field images illustrating the wound closure over 24 hr. (b) A bar graph quantifying the percentage of wound closure
AZ: 5-azacytidine; TR: Trichostatin A; CH: chitosan; Ti: Titanium

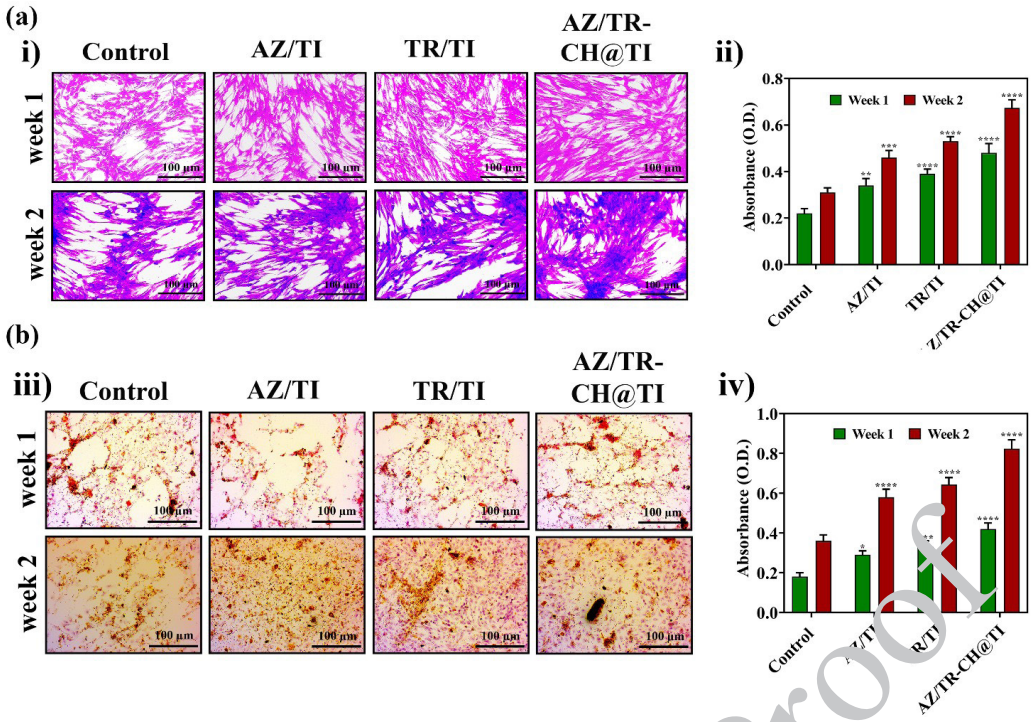

Figure 6. Osteogenic differentiation of MG63 cells on untreated titanium (control), AZ/TI, TR/TI, and AZ/TR-CH@TI composites at weeks 1 and 2, evaluated via (a) ALP and (b) ARS staining
ALP: Alkaline Phosphatase; ARS: Alizarin Red S; AZ: 5-azacytidine; TR: Trichostatin A; CH: chitosan; Ti: Titanium

characterized by an increase in cell body size and a more cuboidal appearance typical of differentiating osteoblasts. The TR/TI group exhibited comparable moderate staining patterns, characterized by distinct purple deposits throughout the cell culture, along with noticeable alterations in cell shape, resulting in a more polygonal morphology. The AZ/TR-CH@TI composite coating exhibited the most significant ALP staining at week 1, characterized by a uniform deep purple coloration throughout the culture area and concentrated nodular formations indicative of active mineralization sites. By the second week, the patterns of osteogenic differentiation were more clearly evident in all groups. The control group exhibited a modest increase in ALP staining, characterized by light to moderate purple coloration and the formation of small cellular aggregates. The AZ/TI and TR/TI groups demonstrated increased staining intensity, characterized by darker purple deposits and a greater formation of multicellular nodules indicative of osteogenic differentiation. The AZ/TR-CH@TI group exhibited optimal osteogenic differentiation, characterized by intense purple staining, extensive nodular formations, and distinct osteoblast morphology, featuring large, polygonal cells arranged in organized patterns. The observed increase in ALP staining intensity and nodule formation from week 1 to week 2, especially in the epigenetic drug-treated groups, indicates an enhanced capacity for osteogenic differentiation and highlights the potential of these coatings to facilitate significant bone formation around TI.

ARS staining

In MG63 cells grown on TI surfaces coated with epigenetic drugs, calcium deposition and mineralization were evaluated using Alizarin Red S staining as markers of progressive osteogenic differentiation (Figure 6b). Microscopic analysis at week 1 revealed that the treatment groups exhibited varying levels of mineral deposition. Limited calcium deposition and early-stage mineralization were indicated by the sparse, light red deposits dispersed throughout the cell culture of the control group (untreated titanium) and negligible ARS staining. There were few indications of matrix mineralization, and the cells retained their characteristic fibroblastic look. The AZ/TI group exhibited noticeable alterations in the extracellular matrix architecture, accompanied by mild red staining and evident calcium deposits that formed small clusters around regions of higher cell density. Comparing the TR/TI group to the control, the former exhibited comparable mild mineralization patterns, characterized by distinct red-stained nodules and enhanced matrix deposition. At week 1, the AZ/TR-CH@TI composite coating exhibited the most noticeable mineralization, characterized by widespread calcium deposition over the culture area, numerous well-formed mineralized nodules, and intense red staining. By week two, all groups' mineralization patterns had significantly improved. The production of tiny mineralized clusters and enhanced but still restricted red staining were signs of moderate improvement in the control group. With bigger mineralized nodules, deeper red deposits, and a broader coverage area of calcium deposition, the AZ/TI and TR/TI groups showed notable improvement. An improved matrix organization with distinctive, bone-like nodular structures was observed under a microscope. The AZ/TR-CH@TI group most astonishingly achieved optimum mineralization, exhibiting the most intense red staining, massive, confluent, nodular formations, a broad covering of mineralized matrix, and distinctive three-dimensional, bone-like structures. The significant rise in calcium deposition from week one to week two, especially

in the groups receiving epigenetic drugs, validated advanced osteogenic differentiation and demonstrated the effectiveness of these coatings in promoting widespread bone mineralization around TI.

AO/EtBr staining

Cell survival and apoptotic patterns in MG63 cells cultivated on titanium surfaces coated with epigenetic drugs over 6 days were evaluated using AO/EtBr dual staining (Figure 7a). All treatment groups exhibited predominantly green fluorescence at day 1, as observed in microscopic examinations, indicating good cell viability with minimal red fluorescence. Indicating typical baseline cell death, the control group had consistent green staining with sporadic red-stained cells and dispersed individual cells. Bright green fluorescence dominated the field in both the AZ/TI and TR/TI groups, showing strong early biocompatibility. Superior cell vitality was demonstrated by the AZ/TR-CH@TI group, which exhibited the most consistent and intense green fluorescence, along with good cell distribution and minimal red fluorescence. By day four, the green fluorescence was still prevalent and the cell density had grown in all groups. Moderate green staining and slightly elevated red fluorescence were seen in the field for the control group. The AZ/TI and TR/TI groups showed fewer apoptotic cells, better cellular structure, and increased green fluorescence. With the strongest green fluorescence and almost no red staining, the AZ/TR-CH@TI group continued to exhibit excellent viability. The viability patterns were more noticeable on day six. In regions of high confluence, the control group sometimes exhibited clusters of red-stained cells, accompanied by excellent green fluorescence. The TR/TI and AZ/TI groups exhibited low cell death and consistent brilliant green fluorescence, accompanied by well-organized cellular structures. The strongest and most consistent green fluorescence throughout the culture, the AZ/TR-CH@TI group most astonishingly showed excellent cell viability, demonstrating remarkable biocompatibility and long-lasting cellular health during the prolonged culture time.

MMP evaluation

The MMP and cellular metabolic activity of MG63 cells grown on titanium surfaces coated with epigenetic drugs were assessed using rhO-123 staining (Figure 7b). Different fluorescence patterns showing the health of the mitochondria in each treatment group were seen under a microscope. Throughout the cell population, the control group's mild green fluorescence was distributed unevenly; some cells showed intense mitochondrial labelling, while others showed low fluorescence, indicating varying metabolic activity. The AZ/TI group exhibited enhanced mitochondrial activity and cellular metabolism, as indicated by increased green fluorescence intensity and a more even distribution across the cell monolayer. Brighter punctate mitochondrial staining patterns, indicative of vigorous cellular respiration, were seen in individual cells. A similar improvement was observed in the TR/TI group, which exhibited unique mitochondrial networks detectable within individual cells, along with enhanced cellular structure and increased fluorescence intensity. Throughout the entire culture area, the AZ/TR-CH@TI composite coating showed the strongest and most consistent green fluorescence, indicating excellent mitochondrial

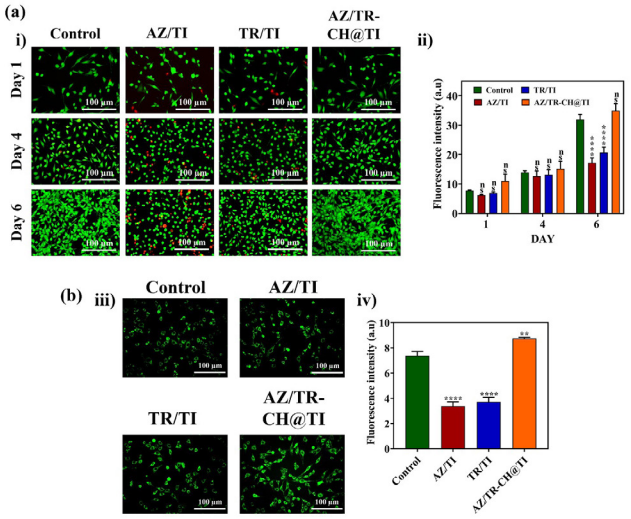

Figure 7. (a) MG63 cell viability over 6 days, featuring (i) representative fluorescence images and (ii) quantitative intensity across treatments (Control, AZ/TI, TR/TI, AZ/TR-CH@TI). (b) Mitochondrial Membrane Potential (MMP) evaluated via (iii) Rho-123 staining and (iv) relative fluorescence intensity, demonstrating superior mitochondrial activity in the AZ/TR-CH@TI composite
AZ: 5-azacytidine; TR: Trichostatin A; CH: chitosan; Ti: Titanium

activity. When compared to the other treatment groups, the cells' remarkable mitochondrial staining, brilliant, well-organized mitochondrial networks, and distinctive perinuclear distribution patterns demonstrated greater cellular metabolic activity and mitochondrial health.

ROS estimation

To assess intracellular ROS levels and oxidative stress in MG63 cells grown on titanium surfaces coated with epigenetic drugs, DCFH-DA staining was used (Figure 8a). Different light patterns reflecting cellular oxidative state were seen under a microscope in each treatment group. The cell population in the control group exhibited a heterogeneous distribution of moderate to high green fluorescence, with many cells displaying brilliant fluorescent signals that indicated oxidative stress and elevated ROS levels. A significant buildup of reactive oxygen species was indicated by the strong cytoplasmic fluorescence and sporadic nuclear staining observed in individual cells. In contrast to the control group, the AZ/TI group showed less intense green fluorescence, with a more even and subdued distribution of fluorescence across the cell monolayer, suggesting a lower degree of oxidative stress. With significantly lower fluorescence intensity and improved cellular appearance, the TR/TI group exhibited a comparable decrease in ROS levels. Most cells also displayed less cytoplasmic fluorescence. Throughout the whole culture area, the AZ/TR-CH@TI composite coating showed the lowest fluorescence intensity and the best ROS control. In contrast to the other treatment groups, the cells showed little to no green fluorescence, clean cytoplasm, distinct cellular borders, and a typical healthy cellular shape, all of which indicated better antioxidant protection and less oxidative stress.

Real-time gene expression analysis

Quantitative real-time PCR was conducted to assess the expression levels of inflammatory and osteogenic genes in MG63 cells cultured on titanium surfaces coated

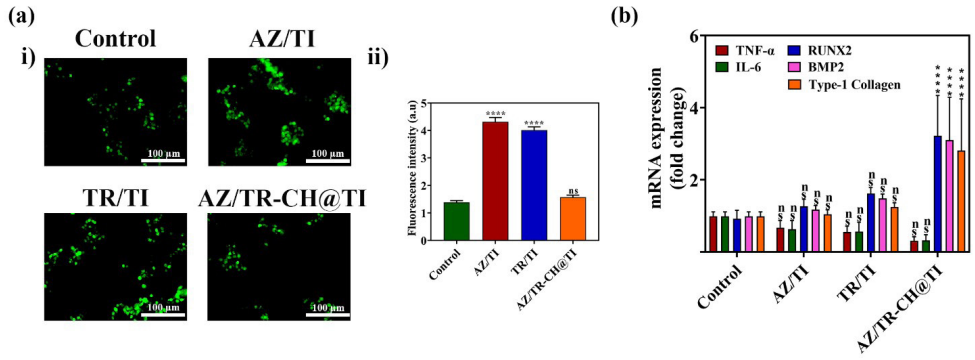

Figure 8. (a) Intracellular reactive oxygen species (ROS) Levels in MG63 Cells Cultured on AZ/TI, TR/TI, AZ/TR-CH@TI composites. (i) Representative microscopic images show the green fluorescence intensity, which is indicative of ROS levels, in cells cultured on different titanium coatings. (ii) A quantitative analysis of the fluorescence intensity demonstrates the relative ROS levels across the treatment groups, including Control, AZ/TI, TR/TI, and AZ/TR-CH@TI. (b) Relative gene expression of inflammatory (TNF-α, IL6) and osteogenic (RUNX2, BMP2, Type-1 collagen) genes in MG63 cells cultured on different titanium surfaces
AZ: 5-azacytidine; TR: Trichostatin A; CH: chitosan; Ti: Titanium

with epigenetic drugs (Figure 8b). Gene expression was normalized to the control (untreated titanium), with a fold change of 1.0 set as the reference. TNF-α expression exhibited significant down-regulation in all treatment groups relative to the control group. The AZ/TI group showed an expression level of 0.67±0.08-fold (P<0.01), whereas the TR/TI group exhibited a 0.59±0.06-fold expression (P<0.001). The AZ/TI-CH formulation demonstrated increased anti-inflammatory effects with a 0.43±0.05-fold expression (P<0.0001), while the AZ/TR-CH@TI composite reached optimal suppression at 0.31±0.04-fold expression (P<0.0001). IL6 expression was significantly reduced with AZ/TI at 0.71±0.09-fold (P<0.05), TR/TI at 0.62±0.07-fold (P<0.01), AZ/TI-CH at 0.48±0.06-fold (P<0.001), and AZ/TR-CH@TI demonstrating maximum suppression at 0.35±0.05-fold (P<0.0001). In contrast, osteogenic markers exhibited notable up-regulation. RUNX2 expression exhibited a progressive increase with AZ/TI at 1.28±0.2-fold (P<0.01), TR/TI at 1.62±0.28-fold (P<0.001), and AZ/TR-CH@TI achieving optimal expression at 2.60±0.47-fold (P<0.0001). BMP2 expression showed comparable increases with AZ/TI at 1.18±0.24-fold, TR/TI at 1.51±0.29-fold, and AZ/TR-CH@TI at 2.2±0.41-fold (P<0.0001). Type-1 collagen expression exhibited a progressive up-regulation with AZ/TI at 1.0±0.1-fold, TR/TI at 1.28±0.25-fold, and AZ/TR-CH@TI achieving maximum expression at 3.04±0.26-fold (P<0.0001). The gene expression profiles validated the dual therapeutic effect of epigenetic drug coatings, which concurrently inhibit inflammatory responses and promote osteogenic differentiation, with the composite coating exhibiting optimal therapeutic potential.

Immunofluorescence staining of osteogenic markers

Immunofluorescence staining was performed to evaluate the expression of key osteogenic markers, including OPN, OCN, ALP, and RUNX2, in MG63 cells cultured on titanium surfaces treated with epigenetic drugs (Figure 9). Microscopic observations revealed distinct fluorescence

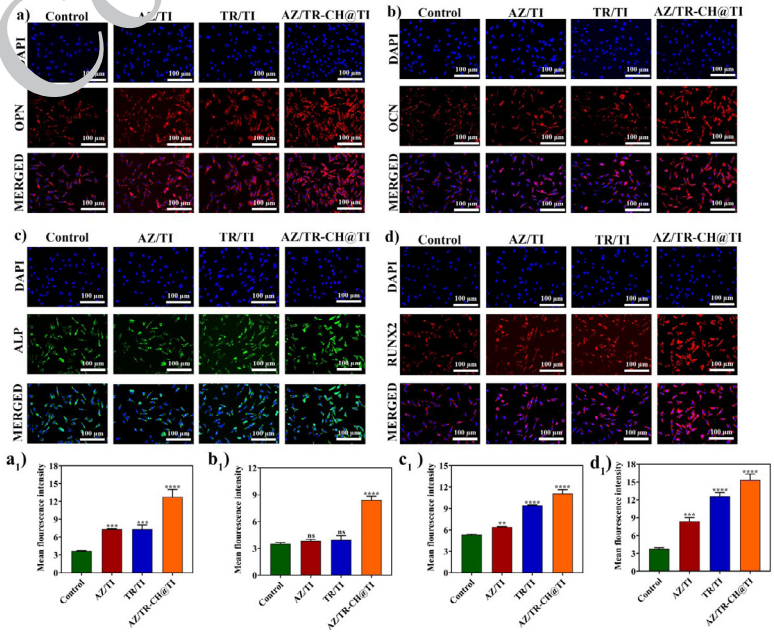

Figure 9. Immunofluorescence staining of osteogenic markers in MG63 cells
Representative images show the expression of (a) OPN, (b) OCN, (c) ALP, and (d) RUNX2 in MG63 cells cultured on different titanium surfaces. Mean fluorescence intensity (a1) OPN, (b1) OCN, (c1) ALP, and (d1) RUNX2. Note: The specific surface treatments correspond to the control, AZ/TI, TR/TI, and AZ/TR-CH@TI groups. Scale bar: 100 µm
OPN: Osteopontin; OCN: Osteocalcin; ALP: Alkaline Phosphatase; RUNX2: Runt-related Transcription Factor 2; AZ: 5-azacytidine; TR: Trichostatin A; CH: chitosan; Ti: Titanium

patterns, indicating the osteogenic differentiation status among the treatment groups. The control group exhibited weak to moderate fluorescence across all markers, with a heterogeneous distribution. OPN exhibited scattered cytoplasmic staining (Figure 9 a, a_1), OCN showed minimal perinuclear fluorescence (Figure 9 b, b_1), ALP indicated weak cellular distribution (Figure 13 c, c_1), and RUNX2 presented dim nuclear localization (Figure 9 d, d_1). The AZ/TI group exhibited increased fluorescence intensity for all markers relative to the control, with enhanced OPN cytoplasmic distribution, elevated OCN perinuclear staining, intensified ALP cellular expression, and more significant RUNX2 nuclear accumulation. The TR/TI group exhibited comparable enhancement, characterized by significantly elevated marker expression, particularly pronounced ALP staining and increased RUNX2 atomic translocation. The AZ/TR-CH@TI composite coating exhibited optimal marker expression, showing the highest fluorescence intensity for all proteins. Cells demonstrated notable OPN cytoplasmic organization, significant OCN perinuclear localization, and widespread ALP distribution in the cytoplasm. They pronounced RUNX2 nuclear accumulation, suggesting enhanced osteogenic differentiation and increased bone formation potential relative to all treatment groups.

Discussion

The successful development of the coatings was confirmed using FTIR and SEM investigations. The detected peak shifts in FTIR spectra signify intermolecular interactions among the epigenetic medicines, CH, and the titanium surface, implying the establishment of a stable coating facilitated by hydrogen bonding and coordination interactions (38-40). The CH matrix is essential for coating stability, as its amino and hydroxyl functional groups engage with the titanium oxide layer to provide a bioactive interface that facilitates drug retention and cellular interaction.

SEM investigation demonstrated a porous and linked microarchitecture, advantageous for drug loading and cellular infiltration. The CH coating alters the surface properties of inert titanium, improving surface wettability and facilitating integrin-mediated cell adhesion and osteoblast proliferation, in accordance with other studies (41).

A significant characteristic of the coating system is its pH-responsive drug release mechanism under inflammatory circumstances (pH 5.5), facilitating localized and condition-specific drug delivery at inflamed implant locations (42, 43). In contrast to traditional titanium surface treatments that provide restricted temporal regulation of bioactive molecule delivery (44), the current method exhibited prolonged drug release exceeding 48 hr. This extended exposure is especially pertinent during the early post-implantation phase, when cellular adhesion, proliferation, and differentiation processes are at their peak activity.

The simultaneous administration of AZ and TR creates a local biochemical environment that is functionally aligned with the concurrent modification of DNA methylation and histone acetylation pathways. Although AZ and TR are recognized inhibitors of DNA methyltransferases and histone deacetylases, respectively, this work did not explicitly evaluate DNA methylation status, histone acetylation levels, or chromatin occupancy at specific gene loci. The observed elevations in osteogenic markers, such as RUNX2 (5.42-fold), BMP2, and type I collagen, are construed as biological consequences of epigenetic regulation, rather than direct indicators of chromatin remodeling (45, 46).

The elevated cell viability (124.6%) reported for the AZ/TR-CH coating suggests that the chosen concentrations (2.5 μM AZ and 100 nM TR) confer biological activity without causing cytotoxicity, corroborating the hormetic dose–response relationship previously shown for epigenetic modulators. The transition from early osteogenic markers (ALP) to late-stage mineralization (ARS) indicates persistent osteogenic commitment; nevertheless, direct validation of durable epigenetic alterations necessitates further molecular investigations (47).

In addition to osteogenic enhancement, the coating significantly reduced inflammatory mediators (TNF-α and IL-6), addressing a major clinical challenge associated with titanium implant failure (48). The simultaneous decrease in intracellular ROS levels and stabilization of mitochondrial membrane potential signifies enhanced cellular redox equilibrium and metabolic well-being. These effects align with previous studies connecting epigenetic medication exposure to modified inflammatory and oxidative stress responses; however, the precise chromatin-level processes underpinning these findings have yet to be elucidated (49).

Notwithstanding these encouraging *in vitro* results, some limitations must be recognized. The research excluded direct epigenetic profiling methods, including global or promoter-specific DNA methylation analysis, histone modification measurement, and chromatin immunoprecipitation assays. Thus, mechanistic conclusions on chromatin remodeling are derived from known pharmacological activities and resultant cellular effects instead of direct molecular evidence. Moreover, the sole dependence on *in vitro* models constrains physiological interpretation. Subsequent research involving epigenetic profiling and *in vivo* validation, such as micro-CT and histological evaluation of bone–implant contact, will be crucial to substantiate the mechanistic foundation and translational significance of this coating system.

Conclusion

Our research suggests that epigenetic drug-loaded CH coatings on TI provide a viable approach for simultaneously promoting osteogenesis and inhibiting inflammation. The dual-drug composite coating (AZ/TR-CH@TI) demonstrated optimal performance in all assessed parameters, indicating synergistic effects between AZ and TR. The combination of sustained and controlled drug release with high biocompatibility and significant osteogenic enhancement suggests that this method may serve as an effective clinical solution for enhancing osseointegration of TI. Subsequent investigations must prioritize *in vivo* validation and the optimization of drug loading parameters to facilitate clinical translation.

Acknowledgment

None.

Authors' Contributions

R S contributed to conceptualization, data curation, methodology, software analysis, validation, visualization, writing the original draft, review, and editing; M N and K J performed conceptualization, data curation, visualization, writing the original draft, review, and editing; V D helped

with data curation, validation, visualization, writing the original draft, review, and editing; S K performed conceptualization, data curation, formal analysis, funding acquisition, investigation, methodology, supervision, validation, writing the original draft, review, and editing.

Conflicts of Interest

The authors certify that they possess no recognized competing financial interests or personal affiliations that might have seemingly affected the work presented in this study.

Declaration

We have not used any AI tools or technologies to prepare this manuscript.

References

1. Che Z, Sun Q, Zhao Z, Wu Y, Xing H, Song K, *et al.* Growth factor-functionalized titanium implants for enhanced bone regeneration: A review. Int J Biol Macromol 2024; 274: 133153.
2. Lee H, Shin DY, Bang SJ, Han G, Na Y, Kang HS, *et al.* A strategy for enhancing bioactivity and osseointegration with antibacterial effect by incorporating magnesium in polylactic acid based biodegradable orthopedic implant. Int J Biol Macromol 2024; 254: 127797.
3. Emam SM, Moussa N. Signaling pathways of dental implants' osseointegration: a narrative review on two of the most relevant; NF-κB and Wnt pathways. BDJ Open 2024; 10: 29.
4. Amengual-Penafiel L, Córdova LA, Jara-Sepúlveda MC, Branes-Aroca M, Marchesani-Carrasco F, Cartes-Velásquez R. Osteoimmunology drives dental implant osseointegration: A new paradigm for implant dentistry. Jpn Dent Sci Rev 2021; 57: 12-19.
5. Xiao Y, Ding Y, Zhuang J, Sun R, Sun H, Bai L. Osteoimmunomodulation role of exosomes derived from immun cells on osseointegration. Front BioengBiotechnol 2022; 10: 989537.
6. Trindade R, Albrektsson T, Galli S, Prgomet Z, Tengvall P, Wennerberg A. Osseointegration and foreign body reaction: Titanium implants activate the immune system and suppress bone resorption during the first 4 weeks after implantation. Clin Implant Dent Relat Res 2018; 20: 82-91.
7. Chen L, Guo Z, Duan G, Zhao G, Liu X, Wan Z, *et al.* The multifaceted biomimetic titanium implant promotes bone integration with sequential antibacterial and immune modulation properties. Bioact Mater 2025; 51: 494-511.
8. Zhang H, Wu Z, Wang Z, Yan X, Duan X, Sun H. Advanced surface modification techniques for titanium implants: A review of osteogenic and antibacterial strategies. Front BioengBiotechnol 2025; 13: 1549439.
9. Salvi GE, Bosshardt DD, Lang NP, Abrahamsson I, Berglundh T, Lindhe J, *et al.* Temporal sequence of hard and soft tissue healing around titanium dental implants. Periodontol 2015; 68: 135-152.
10. Jemat A, Ghazali MJ, Razali M, Otsuka Y. Surface modifications and their effects on titanium dental implants. BioMed Res Int 2015; 2015: 791725.
11. Iyer SS. Epigenetic regulation of bone healing: Implications for fracture repair and clinical treatment strategies. Yale J Biol Med 2025; 98: 159.
12. Dashti P, Lewallen EA, Gordon JA, Montecino MA, Davie JR, Stein GS, *et al.* Epigenetic regulators controlling osteogenic lineage commitment and bone formation. Bone 2024; 181: 117043.
13. Zhou GS, Zhang XL, Wu JP, Zhang RP, Xiang LX, Dai LC, *et al.* 5-Azacytidine facilitates osteogenic gene expression and differentiation of mesenchymal stem cells by alteration in DNA methylation. Cytotechnology 2009; 60: 11-22.
14. Sacramento CM, Assis RI, Saito MT, Della Coletta R, da Rocha Dourado M, Sallum EA, *et al.* BMP-2 and asporin expression regulate 5-aza-dC-mediated osteoblast/cementoblast differentiation of periodontal dental ligament mesenchymal progenitor cells. Differentiation 2022; 124: 17-27.
15. Li Q, Liu F, Dang R, Feng C, Xiao R, Hua Y, *et al.* Epigenetic modifier trichostatin A enhanced osteogenic differentiation of mesenchymal stem cells by inhibiting NF-κB (p65) DNA binding and promoted periodontal repair in rats. J Cell Physiol 2020; 235: 9691-9701.
16. Zhou Z, Jiang W, Yan J, Liu H, Ren M, Li Y, *et al.* Trichostatin A enhances the titanium rods osseointegration in osteoporotic rats by the inhibition of oxidative stress through activating the AKT/Nrf2 pathway. Sci Rep 2023; 13: 22967.
17. Kouchak M, Ameri A, Basireh Naseri, and Boldaji SK. Chitosan and polyvinyl alcohol composite films containing nitrofurazone: preparation and evaluation. Iran J Basic Med Sci 2014; 17: 14-20.
18. Seyyed Tabaei SJ, Rahimi M, Akbaribazm M, Ziai SA, Sadri M, Shahrokhi SR, *et al.* Chitosan-based nano-scaffolds as antileishmanial wound dressing in BALB/c mice treatment: Characterization and design of tissue regeneration. Iran J Basic Med Sci 2020; 23:788–799.
19. Krishna VS, Subashini V, Hariharan A, Chidambaram D, Raaju A, Gopichandran N, *et al.* Role of crosslinkers in advancing chitosan-based biocomposite scaffolds for bone tissue engineering: A comprehensive review. Int J Biol Macromol 2024; 283: 137625.
20. Lavanya K, Chandran SV, Balagangadharan K, Selvamurugan NJ. Temperature-and pH-responsive chitosan-based injectable hydrogels for bone tissue engineering. Mater SciEng C 2020; 111: 110862.
21. Kunrath MF, Garnicoa-Pazmino C, Giraldo-Osorno PM, *et al.* Implant surface modifications and their impact on osseointegration and peri-implant diseases through epigenetic changes: A scoping review. J Periodontal Res 2024; 59: 1095-1114.
22. Ashrad F, Pelanyte G, Philip J, Dahlin C, Larsson L. The role of epigenetic functionalization of implants and biomaterials in osseointegration and bone regeneration — a review. Molecules 2020; 25: 5879.
23. Jacob J, van Loosen QC, van den Berg van Saparoea ACH, *et al.* Bridging bioengineering and epigenetics: from technical innovations to clinical applications. Epigenetics Commun 2024; 4: 8.
24. Nouri H, Rasoulpoor S, Pourpirali R, Sadeghi-Soureh S, Esmaeilizadeh N, Dadashpour M, *et al. In vitro* expansion of human adipose-derived stem cells with delayed senescence through dual stage release of curcumin from mesoporous silica nanoparticles/electrospun nanofibers. Life Sci 2021; 285: 119947.
25. Dadashpour M, Kalavi S, Abri A, Zarghami N, Amandi AF. Long-term proliferation and delayed senescence of bone marrow-derived human mesenchymal stem cells on metformin co-embedded HA/Gel electrospun composite nanofibers. J Drug Deliv Sci Technol 2023; 80: 104071.
26. Dadashpour M, Firouzi-Amandi A, Abri A, Alivirdiloo V, Alipourfard I, Raji-Amirhasani A, *et al.* Sustained *in vitro* delivery of metformin-loaded mesoporous silica nanoparticles for delayed senescence and stemness preservation of adipose-derived stem cells. J Drug Deliv Sci Technol 2023; 87: 104769.
27. Dadashpour M, Mousazadeh H, Rahimi Z, Janghorbanian Poodeh R, Asl AN, Akbarzadeh A, *et al.* Preparation and *in vitro* evaluation of cell adhesion and long-term proliferation of stem cells cultured on silibinin co-embedded PLGA/collagen electrospun composite nanofibers. Exp Cell Res 2024; 435: 113926.
28. Nejati K, Mehdi D, Ghareghomi S, Mostafavi E, Ebrahimi-Kalan A, Biglari A, *et al.* GDNF gene-engineered adipose-derived stem cells seeded Emu oil-loaded electrospun nanofibers for axonal regeneration following spinal cord injury. J Drug Deliv Sci Technol 2020; 60: 102095.
29. Sakata R, Minami S, Sowa Y, Yoshida M, and Tamaki T. Trichostatin A activates the osteopontin gene promoter through AP1 site. Biochem Biophys Res Commun 2004; 315: 959-963.
30. Yan X, Ehnert S, Mihaela Culmes, Bachmann A, Seeliger C, Lilianna Schyschka, *et al.* 5-azacytidine improves the osteogenic differentiation potential of aged human adipose-derived

mesenchymal stem cells by DNA demethylation. PloS One 2014; 9: e90846–e90846.
31. Varadhan P, Jayaraman M. Hyalgan-decorated-ferulic acid-loaded pullulan acetate nanoparticles against gastrointestinal cancer cell lines. Emerg Mater 2024; 7: 1115-11127.
32. Lazer LM, Sadhasivam B, Palaniyandi K, Muthuswamy T, Ramachandran I, Balakrishnan A, *et al.* Chitosan-based nano-formulation enhances the anticancer efficacy of hesperetin. Int J BiolMacromol 2018; 107: 1988-1998.
33. Zhao P, Liu H, Deng H, Xiao L, Qin C, Du Y, Shi X. A study of chitosan hydrogel with embedded mesoporous silica nanoparticles loaded by ibuprofen as a dual stimuli-responsive drug release system for surface coating of titanium implants. Colloids Surf B Biointerface 2014; 123: 657-663.
34. Asl SM, Akbari B, Bahraminasab M, Arab S. Unveiling the synergistic influence of TiO 2 and chitosan-based hydrogel in precision surface co-modification for superior pure titanium implant performance. J Biomed Mater Res Part B Appl Biomater 2025; 113: e35605.
35. Aw MS, Khalid KA, Gulati K, Atkins GJ, Pivonka P, Findlay DM, Losic D. Characterization of drug-release kinetics in trabecular bone from titania nanotube implants. Int J Nanomed 2012; 7: 4883-4892.
36. Ordikhani F, Zustiak SP, Simchi A. Surface modifications of titanium implants by multilayer bioactive coatings with drug delivery potential: Antimicrobial, biological, and drug release studies. JOM 2016; 68: 1100-1108.
37. Micheletti C, Suriano R, Grandfield K, Turri S. Drug release from polymer-coated TiO2 nanotubes on additively manufactured Ti-6Al-4V bone implants: A feasibility study. Nano Express 2021; 2: 010018.
38. Geißler S, Barrantes A, Tengvall P, Messersmith PB, Tiainen H. Deposition kinetics of bioinspired phenolic coatings on titanium surfaces. Langmuir 2016; 32: 8050-8060.
39. Wang S, Zhao X, Hsu Y, He Y, Wang F, Yang F, *et al.* Surface modification of titanium implants with Mg-containing coatings to promote osseointegration. ActaBiomater 2023; 169: 19-44.
40. Tardelli JD, Schiavon MA, Dos Reis AC. Chitosan coatings on titanium-based implants-From development to characterization and behavior: A systematic review. CarbohydrPolym 2024; 344: 122496
41. Chen Z, Weng J, Du X, Ji R, Yang X, Yang Y, *et al.* Quaternized chitosan/glycyrrhizic acid co-decorated titanium with enhanced antimicrobial, immunomodulatory, and osteogenic properties for dental implant applications. CarbohydrPolym 2025; 367: 123984.
42. Mu Y, Gong L, Peng T, Yao J, Lin Z. Advances in pH-responsive drug delivery systems. OpenNano 2021; 5: 100031.
43. Yang X, Yang X, Luo P, Zhong Y, Zhang B, Zhu W, *et al.* Novel one-pot strategy for fabrication of a pH-Responsive bone-targeted drug self-frame delivery system for treatment of osteoporosis. Mater Today Bio 2023; 20: 100688
44. Wang S, Zhao X, Hsu Y, He Y, Wang F, Yang F, *et al.* Surface modification of titanium implants with Mg-containing coatings to promote osseointegration. ActaBiomater 2023; 169: 19-44.
45. Li J, Hao L, Wu J, Zhang J, Su J. Linarin promotes osteogenic differentiation by activating the BMP-2/RUNX2 pathway via protein kinase A signaling. Int J Mol Med 2016; 37: 901-910.
46. Zhang P, Tao F, Li Q, Wu S, Fu B, Liu P. 5-Azacytidine and trichostatin A enhance the osteogenic differentiation of bone marrow mesenchymal stem cells isolated from steroid-induced avascular necrosis of the femoral head in rabbit. J Biosci 2019; 44: 87.
47. Liu Y, Zhang XL, Chen L, Li X, Xiong D, Xu F, *et al.* Epigenetic mechanisms of bone regeneration and homeostasis. ProgBiophysMolBiol 2016; 122: 65-72.
48. Eger M, Hiram-Bab S, Liron T, Sterer N, Carmi Y, Kohavi D, *et al.* Mechanism and prevention of titanium particle-induced inflammation and osteolysis. Front Immunol 2018; 9: 2963.
49. Vishnu J, Kasavan P, Shankar B, Dembińska K, SwiontekBrzezinska M, Kaczmarek-Szczepańska B. Engineering antioxidant surfaces for titanium-based metallic biomaterials. J FunctBiomater 2023; 14: 344.